Formation and preferential orientation of Au-free Al/Ti-based ohmic contacts on different hexagonal nitride-based heterostructures

F.Geenen,[1, a)] A. Constant,[2] E. Solano,[1, 3] D. Deduytsche,[1] C. Mocuta,[4] P. Coppens,[2] and C. Detavernier[1, b)]

[1)]*Department of Solid-State Sciences, Ghent University, 9000 Gent, Belgium*

[2)]*ON Semiconductor, Power Technology Centre, Corporate R&D, Oudenaarde, Belgium*

[3)]*Alba Synchrotron Light Source, Cerdanyola del Vallès, Barcelona, Spain*

[4)]*Synchrotron SOLEIL, L'Orme des Merisiers, Saint Aubin BP48, 91192 Gif-sur-Yvette, France*

Wide-bandgap nitride semiconductors are currently in development for high-power electronic applications. Compositional layered heterostructures of such nitrides result in a high polarization field at the interface, enabling a higher electron mobility, a higher power density, and a higher conversion efficiency. Further optimisation of such GaN-based high-electron-mobility transistors (HEMT) can be achieved by evolving from a top $Al_xGa_{1-x}N$ barrier towards AlN or even $In_yAl_{1-y}N$. An ongoing challenge in using such hexagonal nitride semiconductors is the formation of a low-resistive, Au-free, ohmic contact far below $1\,\Omega\cdot$mm. In this paper, we investigate the formation of ohmic contacts by Ti-Al-TiN-based metallization as a function of different annealing temperatures (up to 950 °C), Ti-Al ratios (from 15 up to 35 at.%) and nitride barrier composition ($Al_xGa_{1-x}N$, GaN, AlN, $In_yAl_{1-y}N$). Contacts processed on $Al_xGa_{1-x}N$, GaN and AlN/GaN heterostructures result in low contact resistance of respectively 0.30 and $0.55\,\Omega\cdot$mm, whereas the same contact stack on $In_yAl_{1-y}N$ results in resistance values of $1.7\,\Omega\cdot$mm. **The observed solid-phase reaction of such Ti-Al-TiN stacks were found to be identical for all investigated barrier compositions (e.g. $Al_xGa_{1-x}N$, GaN, AlN and $In_yAl_{1-y}N$), including the preferential grain alignment to the epitaxial nitride layer. The best performing ohmic contacts are formed when the bottom Ti layer is totally consumed and when an epitaxially-aligned metal layer is present, either epitaxial Al (for a contact which is relatively Al-rich and annealed to a temperature below** 660 °C**), or ternary Ti_2AlN (for a relatively Ti-rich contact annealed up to** 850 °C**).** [a] The observation that the solid phase reaction is identical on all investigated nitrides suggests that a further decrease of the contact resistance will be largely dependent on an optimization of the nitride barriers themselves.

[a)] original text: "Independently of the nitride barrier composition (e.g. $Al_xGa_{1-x}N$, GaN, AlN and $In_yAl_{1-y}N$), the best performing ohmic contacts are formed when the bottom Ti layer is totally consumed and when an epitaxially-aligned metal layer is present, either Al for a contact which is relatively Al-rich and which is annealed to a temperature below 660 °C, or ternary Ti_2AlN for a relatively Ti-rich contact annealed up to 850 °C."

[a)]Electronic mail: Filip.Geenen@UGent.be

[b)]Electronic mail: Christophe.Detavernier@UGent.be

I. INTRODUCTION

Power-conversion systems are a crucial segment of the world-wide electric network. Nitride-based semiconductors are currently being developed for innovative power-transistor applications[1]. A nitride-based heterostructure enables high electron mobility and high-voltage compatibility, which results in devices that are far superior to Si-based power transistors.

A nitride-based high-electron-mobility transistor (HEMT) relies on a two-dimensional electron gas (2DEG) that is formed by the spontaneous polarization at the interface between gallium-, aluminium- or indium-nitride-based layers of different composition. Although the state-of-the-art HEMT devices are based upon an $Al_xGa_{1-x}N$/GaN heterostructure, a further improvement can be achieved with $In_yAl_{1-y}N$/GaN or AlN/GaN heterostructures due to a larger polarization field. Unfortunately, the wide band-gap of the top nitride layer such as $Al_xGa_{1-x}N$, AlN or $In_yAl_{1-y}N$ makes it challenging to electrically connect the 2DEG to the source and drain contacts. An increase of Al concentration in the barrier layer of the heterostructure increases the Schottky barrier height which is present at the metal-barrier interface, and it is therefore not straightforward to transfer the metallization scheme from an $Al_xGa_{1-x}N$- or GaN-based technology to AlN or $In_yAl_{1-y}N$-based HEMTs.

Two strategies are required to fully optimise the ohmic contact. Firstly, the contact stack needs to be optimised in terms of composition and production-specific parameters such as annealing temperature. Secondly, the underlying nitride barrier can be modified in order to lower the contact resistance[2] e.g. optimising the barriers' thickness or by fine-tuning the Al- Ga- or In- atomic ratios. For example, Takei et al.[3] demonstrated that the contact resistance depends on the $Al_xGa_{1-x}N$ barrier thickness. However, their study shows that the optimal annealing temperature for each specific $Al_xGa_{1-x}N$ barrier was identical, and that optimal annealing conditions are unaffected by the changes in the barrier. As such, a first step to engineer the optimal contact process conditions can be performed independently of the barrier structure optimisation. However, a question remains whether or not the contact formation alters upon drastically changing the barrier elemental composition (e.g. $Al_xGa_{1-x}N$ versus $In_yAl_{1-y}N$) instead of fine-tuning the atomic ratios.

Therefore, the formation mechanism of low-resistive ohmic contacts needs to be studied with a direct comparison between different nitride-based barriers. The contact formation itself can be influenced by numerous parameters, such as annealing conditions, initial composition of the metal stack and protective capping layer. By consequence, one requires to

control those parameters in order to understand the formation of ohmic contacts.[4]

Nowadays, the most commonly reported contacts stacks on $Al_xGa_{1-x}N$/GaN heterostructures contain elements with a low metal work function such as Ti, Ta or Al.[5,2,6–9]. **These contact stacks require a protective capping layer to prevent out-diffusion and undesired oxidation from the top of the contact stack**[10] . **A large fraction**[11] of the demonstrated low-resistive contacts rely on a Au-based capping layer to avoid oxidation of the contact[9]. However, Au is an undesired contaminant in an industrial Si-CMOS fab. The formation of Au-free ohmic contacts is therefore a critical issue and is of utmost importance for high-volume and low-cost production of HEMT devices in Si-CMOS fabs. Capping layers such as W[12,13] or TiN[6,14,15] therefore are highly interesting candidates for the formation of industrially-relevant ohmic contacts. Alternatively, Ni or Pt as capping layer can also be effective[2,16,17], but these noble metals are also seen as contaminants in Si-CMOS fabs.[18]

We previously reported on the Ti-Al-TiN contact stack[6] for $Al_xGa_{1-x}N$/GaN heterostructures. **We demonstrated that the Ti-Al ratio defines the optimum annealing temperature for ohmic contact formation[6], which confirms earlier insights on similar metal contact schemes**[19,20]. The ratio can be **either** Ti-rich (Ti-to-Al ratio of more than 25 at.%) or Al-rich (Ti-to-Al ratio of less than 25 at.%), a differentiation which is based on the binary Al-Ti phase diagram[21]. **Each Ti-Al ratio corresponds with an optimum annealing temperature**[22]. Ti-rich contacts require an annealing temperature above 850 °C to reach a low contact resistance, whereas Al-rich contacts require an annealing temperature below 600 °C. **Unfortunately, most papers are limited in the number of samples with different Ti-to-Al ratios in the metal stack, or limited in the number of different annealing temperatures (or even limited in both). A study that systematically compares these contact stacks as function of Ti-to-Al ratio, annealing temperature and of the heterostructure barriers would be of great value.**[23] In order to improve our physical understanding of such contacts, this paper reports on the phase transitions of Ti-Al-based contact schemes for contacts between 15 and 35 at.% Ti and for temperatures up to 900 °C and on different nitride barriers.

We first show that the Ti-Al-TiN contact stack can indeed result in low-resistive ohmic contacts on different nitride barriers, although the contact performance is slightly better on $Al_xGa_{1-x}N$- than on AlN- or $In_yAl_{1-y}N$-based heterostructures. We then provide a detailed overview on the observed crystalline phase formation of the different Ti-Al-TiN contact stacks *during* annealing by comparing Al-rich contacts with Ti-rich contacts. **The investigation of the formed crystal struc-**

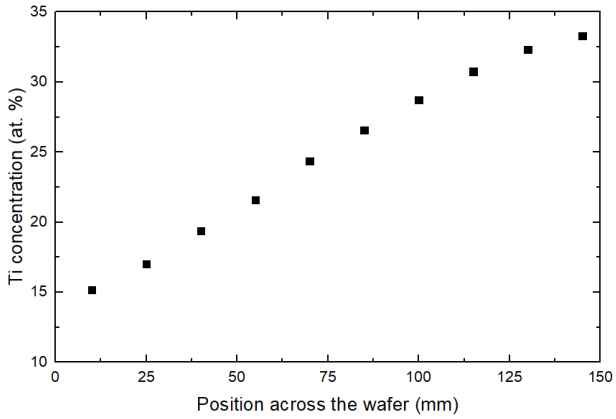

FIG. 1: The Ti concentration of a binary Ti-Al layer monotonously increases as a function of position across the wafer.

tures allows to correlate the contact compositions with the best performing ohmic contacts.[24] Intriguingly, the formed contacts have the same crystalline solid phase reactions and preferential alignment in respect to the epitaxial barriers, independent on that barrier composition. Therefore, the observed differences in electrical performance of the contacts can be attributed to the intrinsic differences of the nitride barrier properties.

II. EXPERIMENTAL

The GaN-based heterostructures were grown on 6-inch, (111)-oriented, Si wafers by metal organic chemical vapour deposition (MOCVD). Several nitride barriers were investigated: $Al_xGa_{1-x}N$, AlN, GaN or $In_yAl_{1-y}N$. An *in situ* grown Si_3N_4 layer was used as a protective capping layer. Ti-Al-TiN contacts were deposited through magnetron sputtering (Physical Vapour Deposition, PVD) on nitride-based heterostructures in two different deposition strategies. The first strategy is a standard PVD deposition of metal stacks with fixed, uniform Ti-Al ratio across the wafer. The thickness of each individual layer was determined by X-ray reflectivity measurements after deposition. These stacks were deposited uniformly on **$Al_xGa_{1-x}N$, AlN, GaN or $In_yAl_{1-y}N$**[25], and capped with a reactively-sputtered protective TiN layer without breaking the vacuum.

A second approach is the PVD deposition of a linear Ti-Al compositional gradient on top of an $Al_xGa_{1-x}N$/GaN-heterostructure wafer. The deposition flux can be tailored by positioning masks in-between the sputter target and the wafer. The deposited layers then have a controlled, linear variation of composition across the wafer[26]. On such a combinatorial gradient, the Ti-to-Al ratio

linearly increases as a function of position on the wafer, as displayed in Fig. 1. As such, metal stacks could be systematically investigated with Ti-Al ratios from 15 up to 35 at. % Ti on a single wafer. This approach enables exploring different compositions in parallel on a single wafer, which enables a cost-effective screening on these expensive substrates and assures identical processing conditions such as chemical cleaning or deposition background pressure for all contacts. These stacks were subsequently capped with a TiN layer without breaking the vacuum.

Both the gradient-deposited wafers as well as uniformly-deposited wafers[27] were then mapped for electrical and morphological properties by optical profilometry (VEECO NT9080 surface profiler) and scanning electron microscopy (SEM) after rapid thermal annealing (RTA) under N_2 ambient at different temperatures for 90 s. The electrical characteristics of the contacts were assessed by transmission line method (TLM) structures from which the ohmic contact resistance (R_c) and the 2DEG sheet resistance (R_{sh}) were extracted.

Lab- and synchrotron-based X-ray diffraction (XRD) measurements were used to investigate the crystal structure of the formed contacts. The first part of our results, section III B, investigates the solid-phase reaction (SPR) of the deposited metal stacks as a function of temperature. The samples were heated at a constant rate of $1\,^{\circ}\mathrm{C\,s^{-1}}$ up to 950 °C in a purified N_2 ambient, while being monitored through XRD using a laboratory setup. A thermocouple installed just below the sample allows to monitor the temperature during the ramp anneal. A CuK_α ($\lambda = 1.54\,\mathrm{nm}$) X-ray source illuminated the sample under a fixed incident angle, while the Bragg diffraction was monitored using a linear detector in a Brucker D8 system, which covered the diffraction angles 2θ from 30 up to 50° (i.e. inter-planar distances from 2.85 down to 1.8Å). As XRD is also an orientation-sensitive technique, the fixed set-up geometry used in these *in situ* measurements will only detect crystal planes which are oriented (nearly) parallel to the sample surface. **This feature was used to avoid over-exposure of the detector due to the highly-intense GaN(002) diffraction peak, by introducing a small out-of-plane tilt of the sample of only a few degrees.**[28] A further numerical improvement of the data's signal-to-noise ratio was achieved by subtracting the minimum intensity recorded by each detector pixel (thus correcting for a constant background intensity originating from e.g. fluorescence).

The fixed-geometry limitations of the *in situ* set-up makes it challenging to study the epitaxial nature of the formed contact phases. The preferential alignment of the contact grains is an important aspect of the microstructure of the ohmic contacts, since it is known that the best ohmic contacts often correspond to an epitaxial alignment[29,30]. *Ex situ* XRD pole figures are therefore a

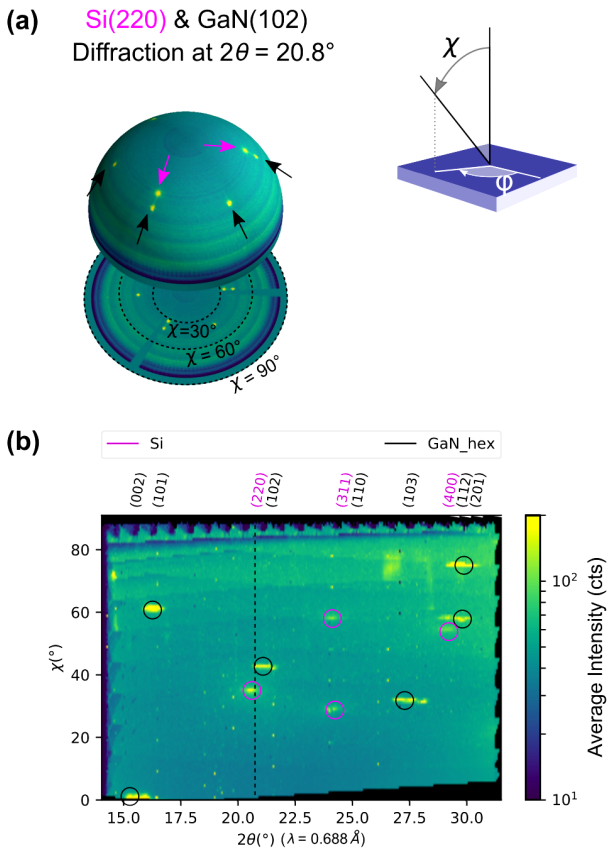

FIG. 2: (Colour on-line) X-ray diffraction intensities of an $Al_xGa_{1-x}N$/GaN heterostructure on top of a Si(111) wafer. **(a)** The diffraction intensities of both Si(220) and GaN(102) planes while tilting the sample both in- and out-of-plane (i.e. azimuth ϕ and elevation χ respectively, see inset) for a fixed incidence and diffraction angles (respectively θ and 2θ). **(b)** The diffraction intensities displayed as a function of both diffraction- and elevation angle (the displayed intensities were averaged along the in-plane, azimuth, tilting angle ϕ).

perfect addition in order to inspect the preferential orientation of the crystal grains. For obtaining an XRD pole figure, the diffracted X-ray signal is recorded while the sample is being tilted and rotated both out-of-plane with respect to the surface normal (defined as the elevation angle χ) and in-plane (azimuth angle ϕ). The **incidence** angle of the X-rays with the sample is set to the value θ, and the angle between the X-rays and the detector is set to 2θ, such that the Bragg law is valid for a desired inter-planer distance d_{hkl}. The resulting dataset is then represented as an intensity map in polar coordinates (Fig. 2a). A high intensity can thus be translated into particular orientations of the corresponding crystalline phase within the probed area of the sample. **XRD-pole figures are able to evaluate the crystalline alignment within the X-ray footprint, e.g. order of**

TABLE I: Crystalline data on the observed epitaxial structures of Si and GaN. Those planes that were observed parallel to Si(111) (i.e. elevation angle $\chi = 0°$) are displayed in **bold**. The diffraction angles for the two different wavelengths used in this article are also displayed.

Compound	Plane	d-spacing (Å)	$2\theta_{in\ situ}$ (°) $\lambda = 1.54$Å	$2\theta_{PF}$ (°) $\lambda = 0.69$Å	Calc. χ angle) (°)
Si	**(111)**	**3.14**	**28.4**	**12.6**	**0**
	(220)	1.92	47.3	20.7	35.3
	(311)	1.64	56.1	24.2	29.5
GaN	**(002)**	**2.59**	**34.5**	**15.3**	**0**
	(101)	2.43	36.8	16.3	62.0
	(102)	1.89	48.1	21.0	43.3
	(103)	1.46	63.4	27.3	32.1
	(100)	2.76	32.4	14.3	90.0
	(110)	1.59	57.8	25.0	90.0

$250 \times 250\,\mu m^2$**, which is an important difference with (high-resolution) transmission electron microscopy (TEM) imaging, which would evaluate the crystalline alignment of a very small area (order of** $100 \times 100\,nm^2$**).**[31]

These *ex situ* XRD measurements were **acquired** at the DiffAbs beamline of the SOLEIL Synchrotron (Gif-sur-Yvette, France)[32]. The incidence X-ray beam was monochromatized using a double-crystal Si(111) monochromator to a wavelength of $\lambda = 0.68\,nm$ (i.e. an energy of $\sim$ 18 keV), with a beam Full Width Half Maximum (FWHM) of $250 \times 250\,\mu m^2$. The sample was mounted on a 6-circles diffractometer (kappa geometry), with a hybrid pixel area detector (XPAD detector[33–36]). The detector was placed so that we were able to measure diffraction angles 2θ between 14 up to 32° (i.e. inter-planar distances from 2.82 down to 1.3Å). The area detector acquired in a so-called *fly-scan* recording mode, acquiring a snapshot every 100 m sec during a continuous in-plane rotation of the samples' azimuth. The use of the area detector enables to acquire diffraction from the full range of χ-values up to 90°, while the sample only needs to rotate for a few discrete steps in the elevation angle of 10°. The discrete step size of 10° in samples' elevation angle renders significant overlap on the area detector of two sequential χ steps. In the following, all the reported diffracting angles 2θ corresponds to the above mentioned X-ray energies, i.e. 0.15

and 0.68 nm for *in situ* laboratory and *ex situ* Synchrotron experiments, respectively.

In the second part of our work (section III C), we discuss the preferential orientation of the crystalline grains directly after deposition and after a RTP-based heat treatment to 400, 500, 600, 700, 800, 900 °C. We display the obtained data in two ways: pole figures show the geometry-dependence for specific diffraction angles **(i.e. specific crystalline planar distance)**, whereas color-intensity plots allow to determine the preferential alignment for a broad range of diffraction angles. Fig 2 shows such plots for a $Al_xGa_{1-x}N$/ GaN reference sample. As Si(111) and $Al_xGa_{1-x}N$ (001) are oriented in the same direction, one can further calculate the expected elevation angles χ **between** different diffraction planes. From these angles, one can derive the alignment of preferentially-oriented crystals, as tabulated in Table II. The supplementary material contains a concise introduction to these plots.

III. RESULTS AND DISCUSSION

A. Electrical performance of ohmic contacts formed on $Al_xGa_{1-x}N$, AlN and $In_yAl_{1-y}N$ barriers

The reported contact resistances R_c of the Ti-Al-based, Au-free, ohmic contacts on $Al_xGa_{1-x}N$ barriers are displayed in Fig. 3 **and includes data from this study as well as literature**[41]. The graph shows that there are two regions of interest (ROI) to obtain low-resistive ohmic contacts on $Al_xGa_{1-x}N$-barriers. Contacts below $1\,\Omega\cdot$mm can be formed either at relatively low temperature, e.g. 550-600 °C, for Ti-to-Al ratios of 15-20 at.%, or after annealing at higher temperature, e.g. 850-950 °C, for 25-35 at.%. We will further discuss the phase formation as a function of Ti-to-Al ratios. Ti-to-Al ratios below 25 at.% will be adressed as *Al-rich*, and Ti concentrations above 25 at.% will be adressed as *Ti-rich*. Our previous work[6] reported that a deviation from these regions-of-interest results in a degradation of the ohmic contact resistance.

Similar to the contacts realized on $Al_xGa_{1-x}N$/GaN heterostructures, Al-rich and Ti-rich contacts were processed on AlN and $In_yAl_{1-y}N$ barriers. It is intriguing that those same contact stacks that result in a low-resistive ohmic contact on $Al_xGa_{1-x}N$ barriers, also perform well on AlN barriers. However, a further improvement to the results can be expected through an optimisation of the barriers, e.g. with recessing (not performed here). Higher contact resistances were measured with metal stacks processed on $In_yAl_{1-y}N$ barriers.

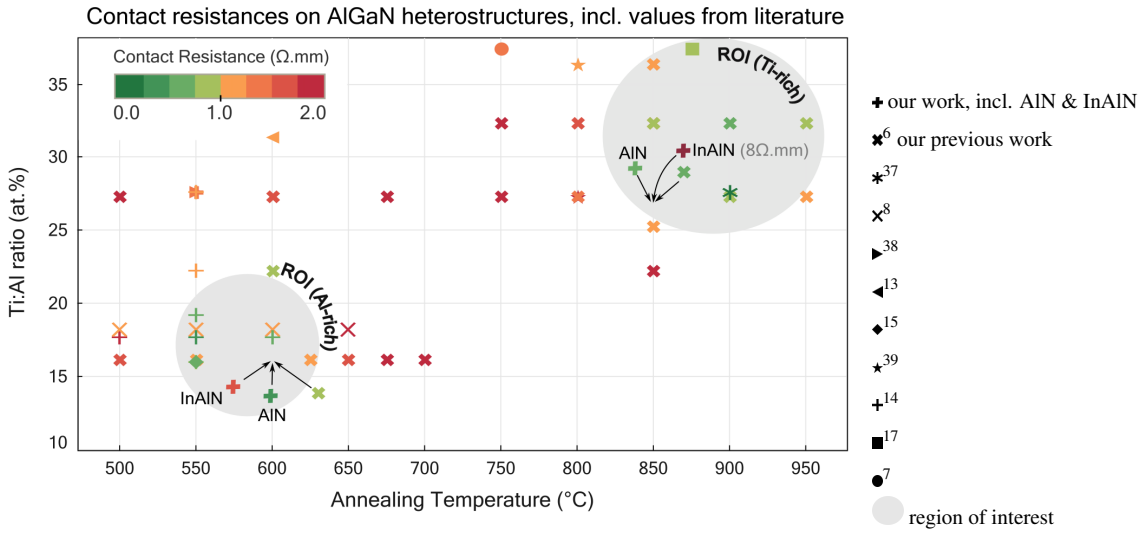

FIG. 3: The average values of contact resistance of Ti-Al-TiN metal stacks with various Ti-Al ratio (excluding the capping layer) and annealing temperatures on $Al_xGa_{1-x}N$ heterostructures. The data shows two regions-of-interest (ROI) in order to form low-resistive ohmic contacts with the Ti-Al-TiN contact scheme on $Al_xGa_{1-x}N$: near 15-20 at.% for 550-600 °C or 25-30 at.% upon annealing up to 850 °C. **This work explored the contact formation within the ROI for InAlN and AlN, as indicated by the arrows.** The shapes of the icons correspond with the origin of the datapoint: **x** our data on $Al_xGa_{1-x}N$[6] and **+** AlN or $In_yAl_{1-y}N$ (this work), ●[7] , ■[17] , +[14], ★[39], ♦[15], ◀[13], ▶[38], ×[8], ∗[37], +[40].

The above classification was further investigated in terms of phase formation, crystal structure and crystal-alignment between the contact stacks and the nitride barriers ($Al_xGa_{1-x}N$, AlN, GaN and $In_yAl_{1-y}N$).[42]

B. Solid phase reaction of Ti-Al-based contacts

A total of 10 different positions were diced out of the deposited Ti-Al-TiN compositional gradient **on the $Al_xGa_{1-x}N$/ GaN heterostructure**, and each sample was measured by *in situ* X-ray diffraction (XRD) during a heating procedure. These measurements allow to identify the phase sequence during the contact formation, and to determine the exact temperatures at which phase transitions are observed. **From these 10 samples, we selected 2 representative measurements to be displayed for respectively 16 and** 29 at.**% Ti (Figs. 4 and 5). These two concentrations are representative for the two main phase sequences observed for the Ti-Al-TiN contact stack.**[43]

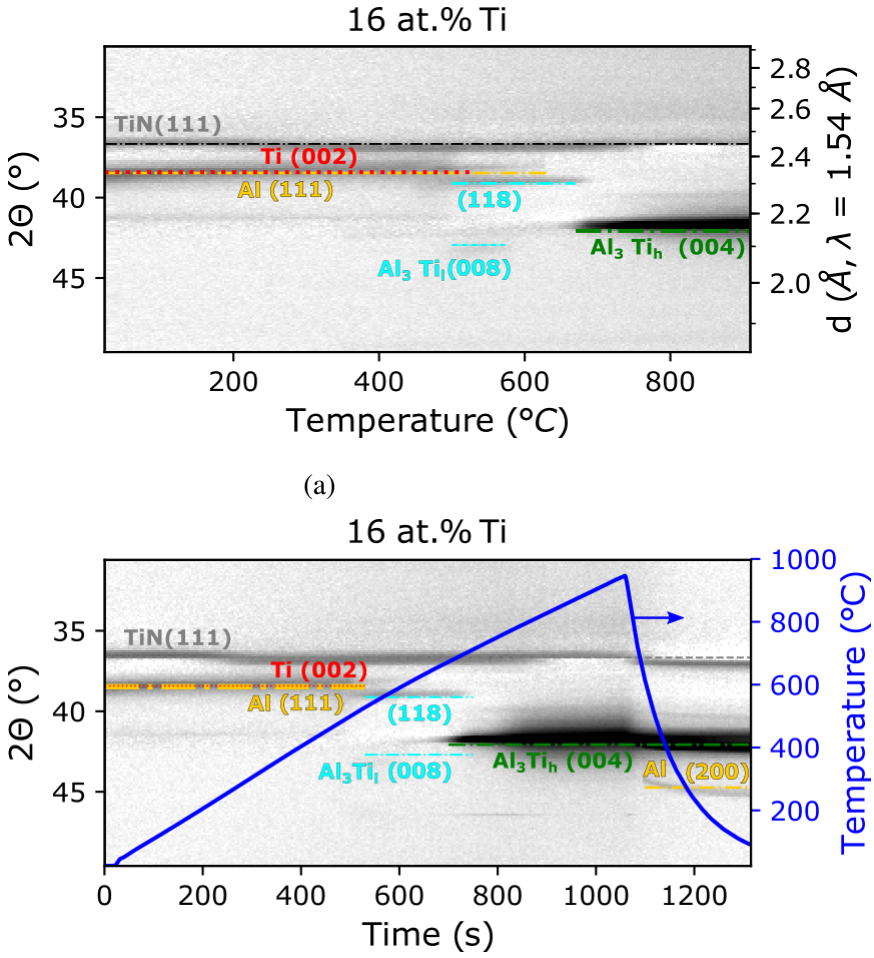

(a)

(b)

FIG. 4: (Colour on-line) *In situ* XRD measurements of a Ti-Al-TiN contact stack with a Ti-to-Al ratio of 16 at.% during annealing as a function of sample temperature (a) or as a function of time (b).

We will start to discuss the phase sequence in detail for these two Ti-to-Al ratios in the coming paragraphs III B 1 and III B 2. Thereafter, a summary is provided on the observed phase sequence for all measured Ti-to-Al ratios in paragraph III B 3. We finalise this section on the solid phase reaction of Ti-Al-TiN contact stacks by comparing the solid phase reaction on different nitride barriers in paragraph III B 4.

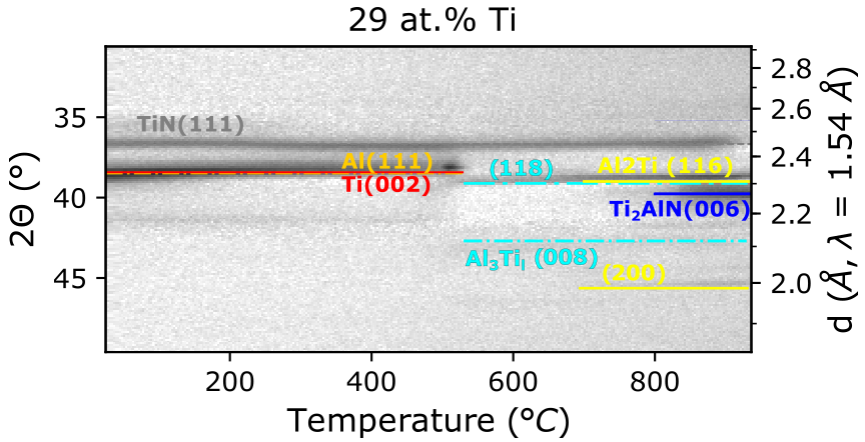

FIG. 5: (Colour on-line) *In situ* XRD measurements of a Ti-Al-TiN contact stack with a Ti-to-Al ratio of 29 at.% during annealing as a function of sample temperature.

*1. Solid phase reaction of an Al-rich metal stack on AlGaN (*16 at.*% Ti)*

The XRD-patterns in Fig. 4 **are displayed as a function of increasing temperature for a sample with Ti-to-Al ratio of** 16 at.**% Ti. At room temperature, two intense XRD peaks are present: a peak near** 2θ=36.8°**, originating from TiN(111), and a peak near** 2θ=38.5°**. The latter can be related to both Ti(002) and Al(111), two crystal planes that have coinciding diffraction peaks due to a similar crystal plane spacing (see also section III C 1 for an in-depth discussion based on XRD pole figures).** [44] The **Ti(002)/Al(111)** diffraction peak remains present up to a temperature of ≈ 665 °C, but already loses half of its intensity at a temperature of ≈ 530 °C. When the Ti(002)/Al(111) diffraction peak has its first major intensity reduction, it is clear from the XRD recording that this is because Ti and Al are consumed in order to form a tetragonal Al_3Ti compound**(as seen by the occurence of it's (118) and (008) peaks)**. As the as-deposited layer contains insufficient Ti to fully convert all the Al into Al_3Ti we can suppose the**remaining** low-intense diffraction peak at 2θ=38.5° can be attributed to the remaining Al above 530 °C. At 660 °C we observe **a complete decline**[45] of this remaining Al(111) diffraction peak, and a new, highly-intense peak arises at 2θ=42.3°, which we correlated to a transformation of the Al_3Ti phase **to the high-temperature variation of the crystal structure**. The tetragonal Al_3Ti phase is known to occur in two different crystal structures with identical stoichiometry[21,46,47], **and is** denoted in this article as a low-temperature (Al_3Ti_l, observed in Fig. 4 below 665 °C) and a high-temperature (Al_3Ti_h, observed in Fig. 4 above 665 °C) structure. The unit cell of Al_3Ti_l can be considered in a first approximation as four stacked unit cells of Al_3Ti_h (with a_l (0.3877 nm)

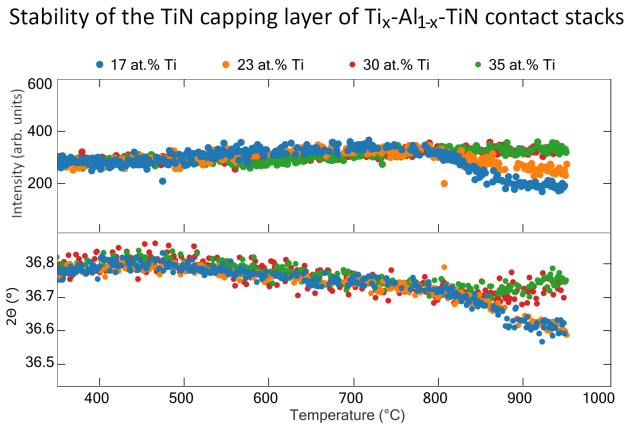

FIG. 6: Evolution of the TiN(111) diffraction peaks' intensity (top panel, arb. units) and diffraction angle during the anneal of samples with different Ti-Al ratios. Lower Ti-concentrations result in an unstable TiN layer, as indicated by the diminishing intensity of the corresponding diffraction signal, as well as diminishing 2θ diffraction angle (i.e. lattice expansion).

$\approx a_h$ (0.3849 nm) and $c_l/4$ (0.8458) $\approx c_h$ (0.8104 nm)). The above observations show that the disappearing Al peak near 660 °C coincides with a significant change in the Al_3Ti crystal structure. Some interesting observations will be made by discussing these measurements more detailed in the following paragraphs.[48]

Firstly, one notices that only few diffraction peaks can be observed for each phase. We will show in paragraph III C that this originates from preferential orientation of these layers. Secondly, it is yet an open question where the excesss of Al reacts into above 660 °C, as there is no sufficient amount of Ti to convert all Al into Al_3Ti. The Ti-Al binary phase diagram[21,46] shows that the Al_3Ti structure is the most Al-rich compound possible, and it is a line phase with a fixed 3:1 ratio of Al to Ti. If elemental Al has not formed a new compound above a temperature of 660 °C, the binary phase diagram suggests that this Al will melt and form a liquid, a material state which is not observable through XRD. Indeed, when the sample cools down after annealing, as seen in Fig. 4b, one does notice that an Al(200) peak appears at $2\theta = 44°$. **This confirms the presence of an Al liquid**[49] at high temperatures which re-solidifies during cooling. **Note that the orientation of the solidified Al after annealing is different from the as-deposited Al in the beginning of the measurement.**[50] Thirdly, the TiN (111) peak of the protective capping layer remains present throughout the measurement, but it's intensity is not constant. Numerical analysis of the XRD

intensities (Fig. 6**, blue curve indicates the currently discussed contact stack**) shows a decline of the TiN (111) diffraction intensity of over 40 % above 800 °C, in favour of an increase in intensity of Al_3Ti. A shift in diffraction angle of TiN(111) is also observed towards lower diffraction angles, i.e. showing that the TiN lattice expands. This **shift in diffraction angle** was previously reported as typical behaviour indicating a transformation towards a more N-rich composition[51,52]. As the Al_3Ti peak is simultaneously increasing in intensity, it indicates that the liquid Al reacts with the capping layer and is partially transformed into Al_3Ti.

Comparing the *in situ* XRD data with the electrical data displayed in Fig. 3 suggests that at 16 at. % Ti, the **region of interest for low-resistive ohmic contacts**[53] is limited due to the melting temperature of Al. **Above this temperature, the contact drastically alters as seen by a change in Al's plane alignment, a transition of Al_3Ti crystal structure and a reduced integrity of the TiN capping layer.**[54].

*2. Solid phase reaction of an Ti-rich metal stack on AlGaN (*29 at*. % Ti)*

For a Ti-to-Al ratio above 25 at. % Ti in the as-deposited stack, we observed a different phase sequence (Fig. 5). The as-deposited diffraction patterns are similar, **and show the presence of Ti, Al and TiN. Now, the presence of Al is limited up to** [55] 538 °C, when Al_3Ti is formed. Near 800 °C, the formed Al_3Ti is accompanied by two other compounds: ternary Ti_2AlN and binary Al_2Ti . A crystal transition of the Al_3Ti phase, which was clearly observable for the lower Ti concentration regime above 660 °C, does not occur: the initial Al_3Ti (118) and (008) peaks are stable throughout the measurement. The high-temperature Ti_2AlN phase only shows the (006)-peak, although the measured range of diffraction angles would also include higher-intensity peaks such as (100) and (103) peaks. Again, this is an indication of crystallographic preferential orientation, i.e. that there is a geometrical link between the epitaxial $Al_xGa_{1-x}N$ substrate and the formed ohmic contacts, which limits the observed orientations of the crystal structures.

From Fig. 5, we can observe that excess of Ti reacts into a combination of Al_3Ti and Al_2Ti so that both Ti and Al are fully consumed. No consumption of the TiN capping layer was observed through any reduction of the diffraction intensity of the TiN(111) peak for these higher Ti concentrations (**red and green lines in** Fig. 6).

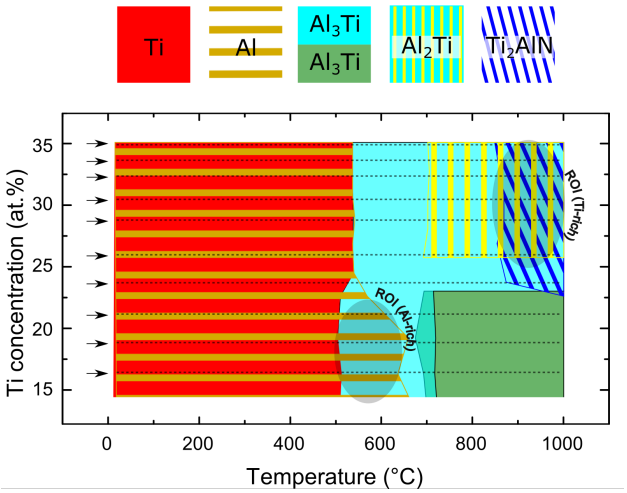

FIG. 7: (Colour on-line) A schematic overview of all crystalline phases as observed through *in situ* XRD **of the Ti-Al-TiN contact stack on an AlGaN/GaN heterostructure**. The average composition of each sample is indicated by a horizontal, dashed, black line at the arrow positions.

3. Solid phase reaction diagram

Similar measurements as discussed above were performed on all other compositions present in the compositional Ti-Al gradient (15 to 35 at. % Ti) **on an AlGaN/GaN heterostructure**. A summary is plotted in Figure 7. The figure allows to identify two different regimes of phase sequence:

- below 25 at. % Ti, also denoted here as an *Al-rich* contact stacks:
  Ti + Al $\rightarrow$ Al_3Ti + Al $\rightarrow$ Al_3Ti + $Al_{liq.}$
- above 25 at. % Ti, also denoted here as an *Ti-rich* contact stacks:
  Ti + Al $\rightarrow$ Al_3Ti+ Ti_2AlN+ Al_2Ti

The observed phases in Fig. 7 illustrate the differences between a bulk phase diagram, which represents the phases in thermal equilibrium at elevated temperatures of the binary Ti-Al system, and the constructed thin-film phase diagram of Ti-Al stacks on an $Al_xGa_{1-x}N$ barrier. The latter shows the phases which are formed during a ramped thermal anneal, and in close proximity of an epitaxial nitride barrier. Similarly to the bulk phase diagram[21,46], one can refer to the atomic composition of the Al_3Ti compound as a reference to define a *Ti-rich* or an *Al-rich* metal stack. A remarkable consequence of the occurrence of these two regimes can be seen by comparing the surface morphology of these contacts after an RTP anneal up to 800 °C. For metal stacks with

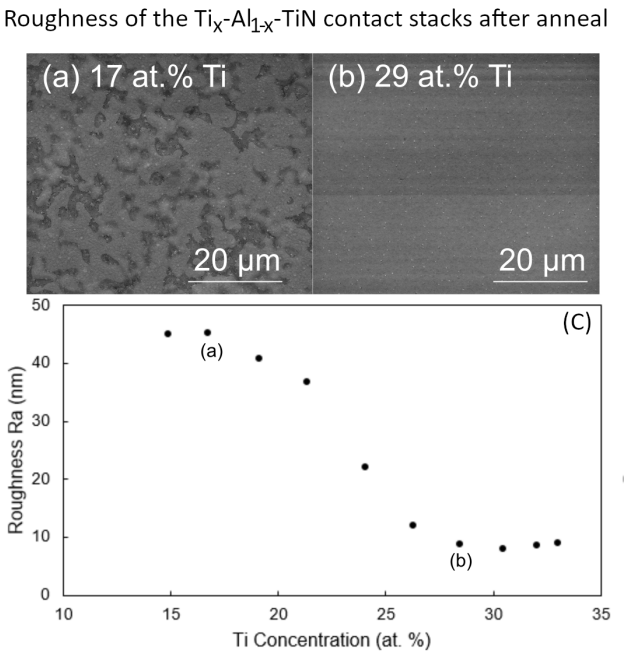

FIG. 8: **Top:** SEM images of the top morphology of the investigated samples show a clearly rougher surface for e.g. Al-rich (point **a**) samples than for Ti-rich samples (point **b**). **Bottom:** *Ex situ* morphology assessment was performed by optical profilometry on samples annealed up to 800 °C and show a drastic change when increasing the Ti concentration above 25 at. %.

an excess of Al, the molten Al re-solidifies during cooling. For such samples, we have observed severe cracks and holes in the surface of the samples (Fig. 8a), while for samples with an excess of Ti, the top surface remains relatively smooth after anneal. In Fig. 8c, the average roughness parameter R_a follows the same two-regime behaviour as observed with the XRD measurements. The roughness is the highest for the lowest Ti concentrations (around 45 nm, but quickly decreases with increasing titanium content, until it converges to a minimum value of $R_a = 8.9$ nm above concentrations of 25 at. % Ti. Previously, Constant et al reported that samples below 25 at. % Ti result in bad contact resistance when annealed at 850 °C, an observation that was correlated with a poor sheet resistivity and morphology[6].

We can then compare the obtained thin-film phase diagram in Fig. 7 with those temperatures and compositional combinations that result in low-resistive contact stacks in Fig. 3. The regions of low ohmic resistance are indeed situated at regions with a unique area on the phase diagram. In the Al-rich regime, low-resistive ohmic contacts are formed for temperatures between 550-600 °C just below the melting temperature of Al. **This corresponds with a temperature window at**

which Ti is already consumed and has formed Al_3Ti and where Al did not yet form a liquid phase[56]. In the Ti-rich regime, low-resistive ohmic contacts are formed when the ternary Ti_2AlN is present.

4. Variation of Nitride barriers

Similar metal stacks of Ti-Al-TiN with relatively low (e.g. 16 at. %) and high (e.g. 26-29 at. %) Ti-to-Al-ratios were deposited on several nitride layers: (hexagonal) $Al_xGa_{1-x}N$, GaN, AlN, $In_yAl_{1-y}N$ and (amorphous) Si_3N_4. The *in situ* XRD measurements on these samples are displayed in Fig. 9, clearly showing that the phase sequence is identical for the same metal stack on different nitride layers, with the sole exception of the depositions on (amorphous) Si_3N_4. Here, no Ti_2AlN (006) peak was observed upon annealing of the Ti-rich contact stack but the (101) peak was observed (at diffraction angle of 35° as seen in a second measurement window, not shown).

C. Crystalline orientation of Ti-Al-based contacts

1. As-deposited metal stack on AlGaN

While discussing the *in situ* XRD measurements, we have noticed that not all diffraction peaks were observed for some compounds. For example, in Fig. 4, one could expect some additional diffraction peaks: Al(200) (d=2.02Å, $2\theta = 44.8°$), TiN(200) (d=2.12Å, $2\theta = 42.6°$), Ti(101) (d=2.24Å, $2\theta = 40.2°$) and Ti(100) (d=2.56Å, $2\theta = 35.0°$). The reason for this peculiarity is related to the measurement geometry of the *in situ* XRD set-up. As the X-ray source, the sample and the detector are in fixed geometry, the set-up only probes those planes which are nearly parallel to the samples' surface. To eliminate this blind spot in our XRD measurements, we have performed 3D XRD color maps for samples annealed to specific temperatures. In Fig. 10, we display the diffraction intensity as a function of diffraction angle 2θ and planar elevation angle χ **(note that the diffraction angle 2θ in our XRD pole figures does not correspond with the diffraction angle from our in-situ XRD, due to a different X-ray wavelength)**. From these plots, we can determine whether a crystal has a random orientation in respect to the substrate**(which results in a vertical line)** or a preferential alignment to the substrate **(which results in a local spot)**.

We can immediately recognise the features related to the Si substrate and the $Al_xGa_{1-x}N$ layers, as indicated by the circles and **which were** previously discussed in the experimental section with

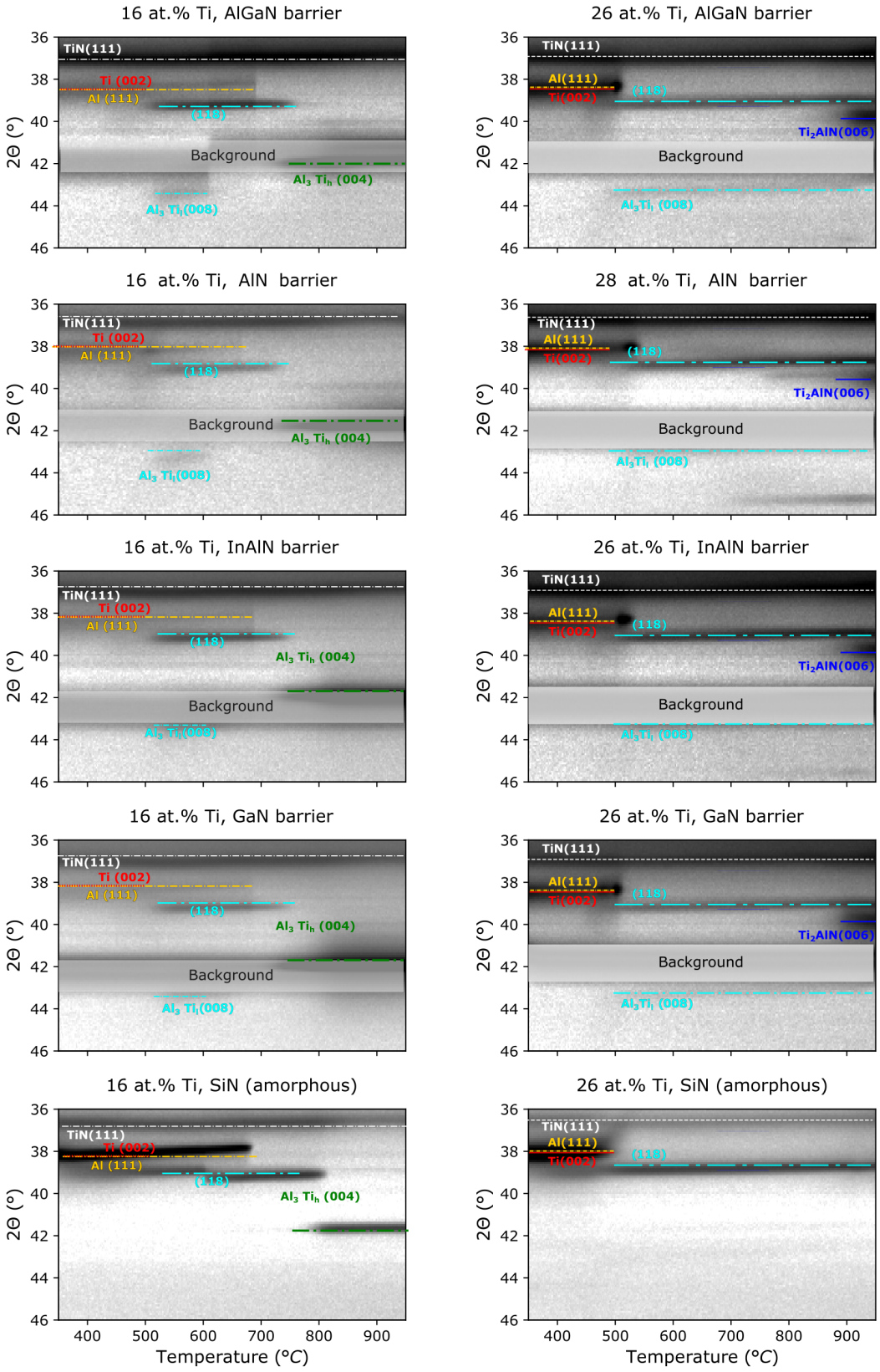

FIG. 9: (Colour on-line) *In situ* XRD measurements of Ti-rich as well as Al-rich contact stacks on different nitride barriers - $Al_xGa_{1-x}N$, AlN, GaN and $In_yAl_{1-y}N$ - and (amorphous) Si_3N_4. For these measurements, there is always an undesired background present due to diffraction of the hexagonal crystalline barrier (AlN, GaN, $In_yAl_{1-y}N$, $Al_xGa_{1-x}N$) by low-intensity W-based

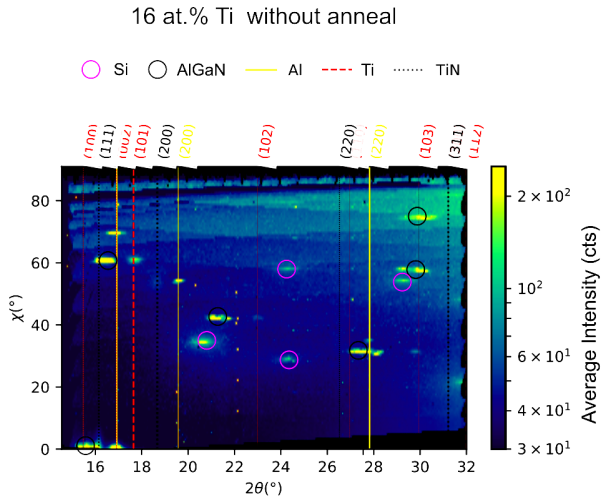

FIG. 10: (Colour on-line) *Ex situ* XRD intensity color maps of a non-annealed Ti-Al-TiN metal stack with Ti-to-Al ratio of 16 at. % as a function of diffraction angle 2θ (λ =0.688 nm) and elevation angle with respect to the substrate surface χ (i.e. the elevation angle). The data clearly shows that Al, Ti and TiN diffraction is only observed for specific values of χ, which is typical behaviour for epitaxial or fibre-textured compounds.

Fig. 2. **The Ti, Al and TiN diffraction patterns are limited at specific values of elevation angle χ, which indicates a preferential orientation of those crystals.**[57] One can then use the known geometry of the crystal unit cells to determine the specific alignment of those crystal grains. For example, if one considers a hypothetical situation where only Al(111) planes are parallel to the samples' surface, then all other crystal planes will **also** have a specific orientation in respect to the samples' surface. **This orientation can be calculated and is equal to the inclination angle with the Al(111) plane, as defined by the crystal structure of Al.**[58] Indeed, the geometric angles between the planes of Al(111) on the one hand and Al(11-1), (200) or (220) on the other hand are respectively 70.5, 54.7 and 35.3° (see also Tab. II). Therefore, if all Al(111) planes are parallel to the samples surface, then e.g. the Al(200) diffraction would only be observed at elevation angle χ = 54.7°, which is the case. Note that this diffraction dataset does not include diffraction of Al at any other χ values, thus eliminating any other orientation for *all* Al grains probed by the X-ray footprint. We can therefore conclude from these measurements that every **compound**[59] in the as-deposited Ti-Al-TiN stack is preferentially aligned with the $Al_xGa_{1-x}N$-barrier.

Two types of preferential orientations are possible: epitaxial-alignment and fibre-alignment. To differentiate between these two alignments, one need to take a closer look to the individ-

TABLE II: Crystalline data on the observed epitaxial structures of as-deposited Ti, Al and TiN. Those planes that were observed parallel to Si(111) (i.e. elevation angle $\chi = 0°$) are displayed in **bold**. The diffraction angles for the two different wavelengths used in this article are also displayed.

Compound	Plane	d-spacing (Å)	$2\theta_{in\ situ}$ (°) $\lambda = 1.54$Å	$2\theta_{PF}$ (°) $\lambda = 0.69$Å	Calc. χ angle (°)
Ti	**(002)**	**2.34**	**38.4**	**16.7**	**0**
	(100)	2.56	35.1	15.3	90
	(101)	2.24	40.2	17.4	61.4
	(102)	1.72	53.0	22.7	42.5
	(103)	1.33	70.6	29.6	31.4
Al	**(111)**	**2.34**	**38.5**	**16.7**	**0**
	(200)	2.02	44.7	19.3	54.7
	(220)	1.43	65.1	27.5	35.3
TiN	**(111)**	**2.45**	**36.6**	**16.0**	**0**
	(200)	2.12	42.6	18.5	54.7

ual pole figures in Fig. 11.[60] Here, we observe that the diffraction of Ti, Al and TiN are also limited in the in-plane angle ϕ-angle, thus showing that the as-deposited layers have an epitaxial alignment. The specific alignments are defined through:

$$Ti(002)//Al_xGa_{1-x}N(002) \quad \& \quad Ti(100)//Al_xGaN1-x(100)$$

$$Al(111)//Al_xGaN1-x(002) \quad \& \quad Al(1-10)//Al_xGaN1-x(100)$$

$$TiN(111)//Al_xGaN1-x(002) \quad \& \quad TiN(1-10)//Al_xGaN1-x(100)$$

These alignments were observed both for as-deposited stacks with 16 and 27 at.% Ti on $Al_xGa_{1-x}N$ barriers, even after an RTP-based anneal up to 400 °C. Those stacks that were annealed up to 500 °C result in different XRD-pole figures and are dependent on the initial Ti-Al ratio, as expected from our *in situ* XRD-based phase identifications.

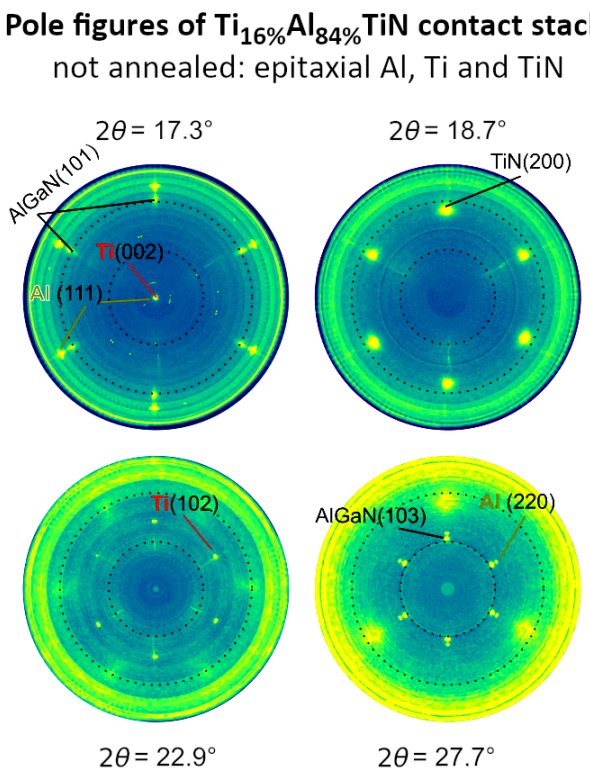

FIG. 11: (Colour on-line) *Ex situ* XRD pole figures of specific diffraction angle 2θ (λ =0.688 nm): 2θ= 17.3° (d = 2.29 Å; contains diffraction from $Al_xGa_{1-x}N$(101), Ti(002) and Al(111)), 2θ= 18.7° (d = 2.12 Å; contains diffraction from TiN(200)), 2θ= 22.9° (d = 1,73 Å; diffraction from Ti(102) and 2θ= 27.7° (d = 1.44 Å;contains diffraction from $Al_xGa_{1-x}N$(103) and Al(220)). The data clearly shows that that Ti, Al and TiN are epitaxially aligned.

2. *Annealed Al-rich metal stacks on AlGaN* (16 at. %)

The XRD pole figures of an Al-rich contact stack with 16 at. % Ti, annealed by RTP up to 600 °C is displayed in Fig. 12. This combination of annealing temperature and Al-concentration is of peculiar interest, as it was previously identified as one of the two regions for formation of low-resistive ohmic contacts. We can again recognise the diffraction peaks related to the single-crystal Si(111) wafer and the $Al_xGa_{1-x}N$/GaN-based heterostructures. The diffraction spots of as-deposited Al are situated at those diffraction angles and elevation angles χ as displayed in table II. In addition to those epitaxial diffraction features, one now can recognise the diffraction of Al_3Ti as a vertical line, i.e. for all values of χ, which indicates that those crystal grains are randomly-aligned. From these measurements, we can now be certain of the assumption previously made in paragraph III B 1, that Ti is first fully consumed and that residual, epitaxial Al remains present up

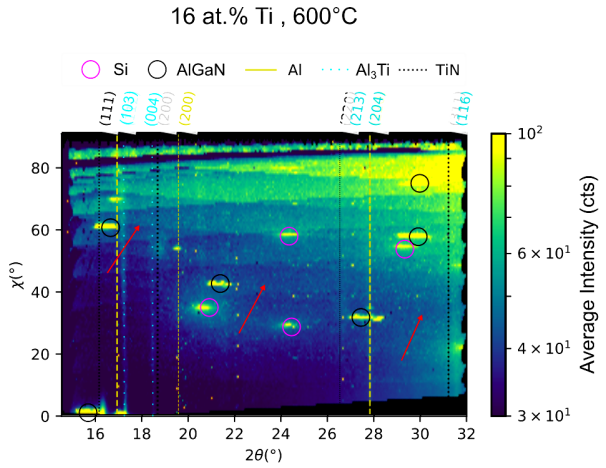

FIG. 12: (Colour on-line) *Ex situ* XRD intensity color maps of a Ti-Al-TiN metal stack with Ti-to-Al ratio of 16 at. % annealed up to 600 °C as a function of diffraction angle 2θ (λ =0.688 nm) and inclination angle with the substrate surface (i.e. the elevation angle χ). The data clearly shows that Al and TiN diffraction is only observed for specific values of χ, which is typical behaviour for epitaxial or fibre-textured compounds. By contrast, Al_3Ti diffraction is observed for all elevation angles χ, which indicates that those crystal grains are randomly-aligned. The red arrows indicate the diffraction positions where Ti was observed for a non-annealed sample.

to it's melting temperature. Therefore, the low-resistive ohmic contact achieved at 600 °C is thus correlated to one, or a combination of, the following conditions:

- the presence of randomly-aligned Al_3Ti
- the consumption of the initial Ti-layer
- the presence of epitaxial layer (epitaxial Al for the Al-rich region)

In section III C 3, we will show that the fullfillment of only the first two conditions does not suffice to form a low-resistive ohmic contact. As such, the third condition seems to be critical to form a low contact resistance in the Al-rich regime. We propose that some reaction with Ti is required in combination with the presence of epitaxial Al[61]. **We speculate that** the reaction of Ti can result in a cleaning at the $Al_xGa_{1-x}N$ barrier, where undesired contaminants are dissolved in solid-solution with Al_3Ti , **or that the reaction of Ti can also** result in out-diffusion of nitrogen from $Al_xGa_{1-x}N$ towards Ti and the formation of Ti–N complex and/or N vacancies in $Al_xGa_{1-x}N$[2].

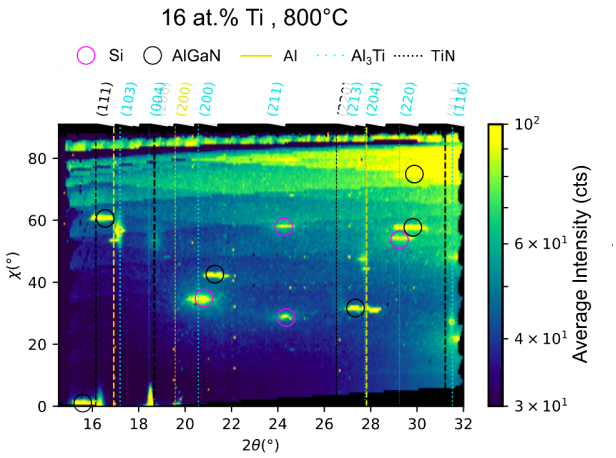

FIG. 13: (Colour on-line) *Ex situ* XRD intensity color maps of a Ti-Al-TiN metal stack with Ti-to-Al ratio of 16 at. % annealed up to 800 °C as a function of diffraction angle 2θ (λ =0.688 nm) and inclination angle with the substrate surface χ (i.e. elevation angle). The data clearly shows that Al, Al_3Ti and TiN diffraction is only observed for specific values of χ, which is typical behaviour for epitaxial or fibre-textured compounds.

When heating an Al-rich sample above the melting temperature of Al, a transformation occurs of Al_3Ti into a different preferential orientation, as shown through pole-figure XRD data in Fig. 13: now the diffraction of the most-intense (103), (004), and (204) peaks of Al_3Ti, which were rather uniform as a function of elevation angle χ in Fig. 12, now have higher diffraction intensities near χ angles of 58°, 0° and 45°, respectively. The diffraction spots of Al are also situated at different elevation angles χ: Al(111), Al(200) and Al(220) diffractions are now limited at χ 54°, 0° and 45°. The crystal alignment of both Al_3Ti and (re-solidified) Al are clearly significantly different from the sample annealed at lower temperatures. An inspection of the individual pole figures in Fig. 14 shows a new crystal preferential orientation, i.e. a fibre-alignment, for which the axis of rotations are determined by:

$$Al(200)//Al_xGa_{1-x}N(002)$$

$$Al_3Ti(004)//Al_xGa_{1-x}N(002)$$

The fibre alignment of Al_3Ti is also evident from a cross-section TEM image of an Al-rich contact in Fig. 15b and c. The planes of the Al_3Ti layer show a clear planar alignment parallel to the surface of the sample after an anneal up to 800 °C, which is not present after an anneal up

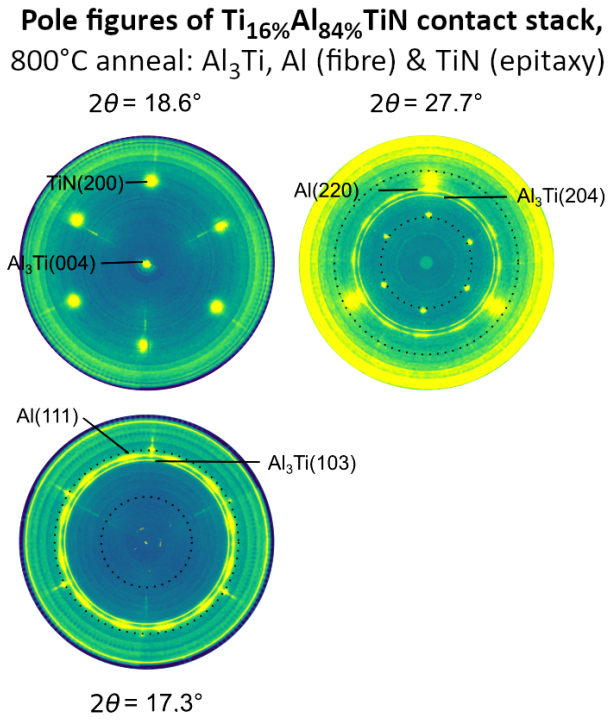

FIG. 14: (Colour on-line) *Ex situ* XRD pole figures of a Ti-Al-TiN metal stack with Ti-to-Al ratio of 16 at. % annealed up to 800 °C at specific diffraction angle 2θ (λ =0.688 nm): 2θ= 18.6° (d = 2.12 Å; contains diffraction from TiN(200), Al_3Ti (004)), 2θ= 17.3° (d = 2.29 Å; diffraction from Al(111) and Al_3Ti (103)) and 2θ= 27.7° (d = 1.44 Å;contains diffraction from $Al_xGa_{1-x}N$(103), Al_3Ti (204) and Al(220)). The concentric circles characteristic to diffracted signal originating from Al and and Al_3Ti shows their fibre-alignment.

to 600 °C. As a fibre alignment does not result in a systematic geometry at the interface between semiconductor and contact, **in contrast to epitaxy,** one can expect that a fibre-aligned contact has poorer contact resistivity values.

3. Annealed Ti-rich metal stacks on AlGaN (27 at. %)

The reciprocal color map of a Ti-rich metal stack with 27 at. % is displayed in Fig. 16 for an RTP-based anneal up to 600 °C and Fig. 17 displays the data after an anneal up to 800 °C. At 600 °C, we observe that the Ti-Al stack has fully converted to randomly-oriented Al_3Ti . **So here we have a situation where the metal stack has formed randomly-aligned Al_3Ti and has consumed the initial Ti-layer. This corresponds with two out of three conditions from section**

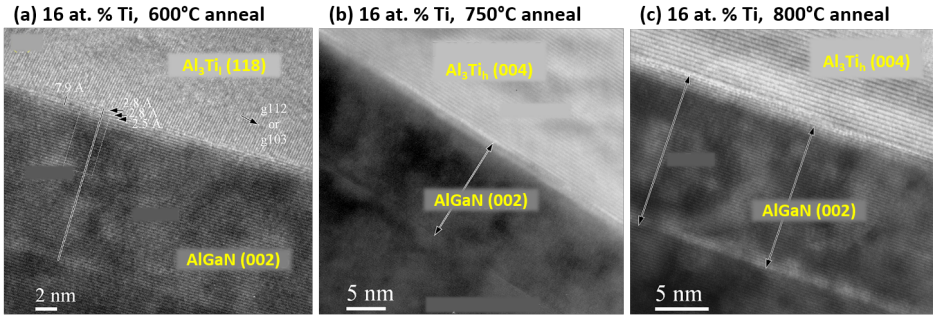

FIG. 15: High-resolution TEM image of a cross section of Al-rich contact (16 at. %) after an RTP-anneal up to **(a)** 600 °C[6] , **(b)** 750 °C and **(c)** 800 °C .

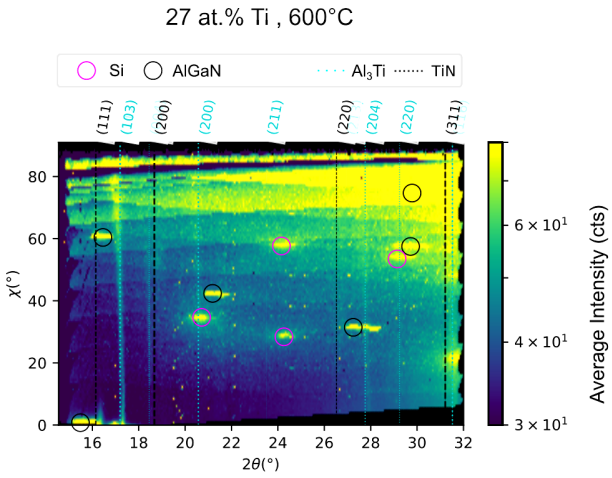

FIG. 16: (Colour on-line) *Ex situ* XRD intensity color maps of a Ti-Al-TiN metal stack with Ti-to-Al ratio of 27 at. % annealed up to 600 °C as a function of diffraction angle 2θ (λ =0.688 nm) and inclination angle with respect to the substrate surface χ (i.e. elevation angle). The data clearly shows that Al_3Ti diffraction is observed for every value of χ, which indicates that those crystal grains are randomly-aligned.

III C 2 that correlated with a low-resistive ohmic contact. As the contact stack here does not result in a low-resistive ohmic contact, it appears that the presence of epitaxial Al is crucial for the contact formation.[62]

At higher temperatures, Fig. 17 shows the formation of Ti_2AlN in addition to this randomly-oriented Al_3Ti . This is also the second region with ideal temperature and compositional conditions for low-resistive ohmic contact. The reciprocal space maps show that Ti_2AlN, which has a hexagonal structure, is epitaxially aligned with the nitride barrier. **The alignment is defined by parallel** a, b and c-axes between Ti_2AlN and $Al_xGa_{1-x}N$, as shown in Fig. 18. Cross-section TEM inves-

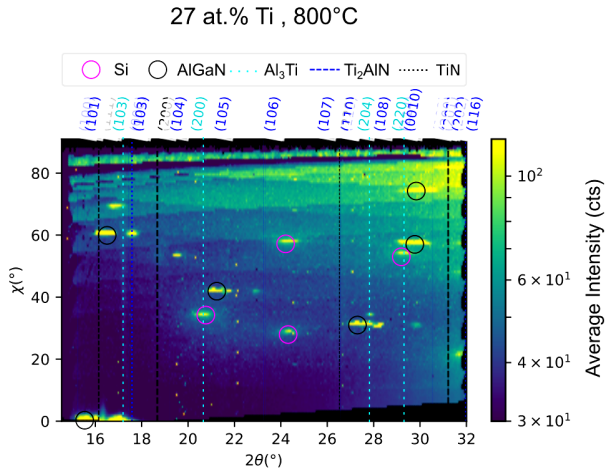

FIG. 17: (Colour on-line) *Ex situ* XRD intensity color maps of a Ti-Al-TiN metal stack with Ti-to-Al ratio of 27 at. % annealed up to 800 °C as a function of diffraction angle 2θ (λ =0.688 nm) and inclination angle with the substrate surface χ. The data clearly shows that Ti_2AlN diffraction is only observed for specific values of χ, which is typical behaviour for epitaxial or fibre-textured compounds.

tigation shows that the Ti_2AlN is formed at the interface between the $Al_xGa_{1-x}N$ barrier and the contact stack (Fig. 19). **Again we observe that the formation of a low-resistive ohmic contact occurs with the presence of randomly-aligned Al_3Ti, the consumption of the initial Ti-layer and with the presence of an epitaxial layer, this time the intermediate Ti_2AlN layer between the barrier and Al_3Ti.** [63]

4. Phase alignment differences between nitride barriers

Pole figure measurements of **a** Al-rich and **a** Ti-rich metal stack was obtained for different barriers: $Al_xGa_{1-x}N$, AlN and GaN. No difference could be observed between the contact stacks in terms of formed compounds and their individual alignment in respect to the underlying barrier. **This includes** the formation of ternary Ti_2AlN even on a pure GaN barrier. As such, we can conclude that not only the phase sequence is identical for the same contact stack on different nitrides, as observed in section III B 4, but also their alignment in respect to the barrier.

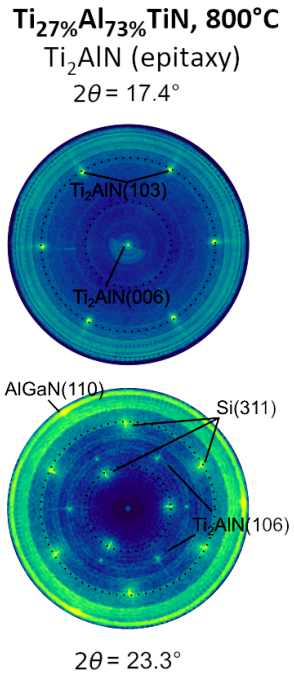

FIG. 18: (Colour on-line) *Ex situ* XRD pole figures of a Ti-Al-TiN metal stack with Ti-to-Al ratio of 27 at. % annealed up to 800 °C at specific diffraction angle 2θ (λ =0.688 nm): 2θ= 17.4° (d = 2.28 Å; contains diffraction from Ti_2AlN(103) and (006)) and 2θ= 23.3° (d = 1.71 Å; diffraction from Si(311), $Al_xGa_{1-x}N$(110) and Ti_2AlN(106)).

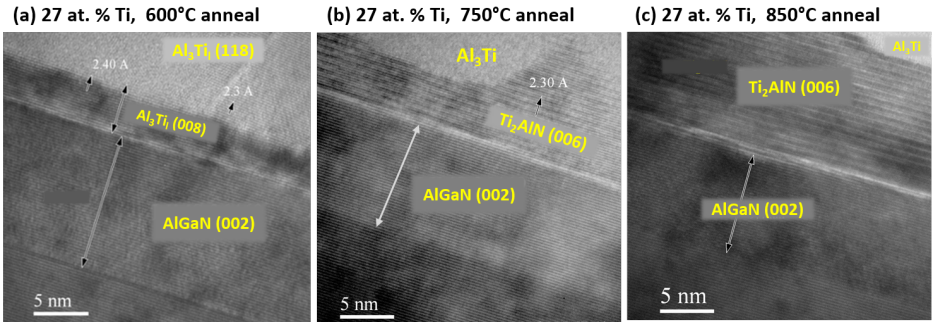

FIG. 19: High-resolution TEM image of a cross section of Ti-rich contact (27 at. %) after an RTP-anneal up to **(a)** 600 °C[6] , **(b)** 750 °C and **(c)** 850 °C[6].

IV. SUMMARY AND CONCLUSIONS

This work compares the formation mechanism of ohmic contacts with different Ti-Al ratios as well as on different nitride barriers. Two optimal zones were identified as a function of annealing temperature as well as Ti-to-Al ratio: 600 °C for Ti concentrations below 25 at. % and

above 850 °C for Ti concentrations above 25 at. %. Remarkable is that these contact stacks also result in low-resistive ($< 1\,\Omega \cdot$ mm) ohmic contacts on other barriers such as AlN. In-depth investigation was performed of the solid phase reaction of the annealed contact stack with different initial Ti-Al compositions. Our X-ray based investigation **for several representative Ti-to-Al ratios** showed that the phase sequence is identical on the different nitride barriers ($Al_xGa_{1-x}N$, GaN, AlN, $In_yAl_{1-y}N$). The preferential orientation of the formed crystalline grains shows that the epitaxial or fibre alignment of the formed ohmic contacts are identical for the different nitride barriers, as observed by full-reciprocal space XRD pole figures . The best performing contact stacks coincides with the following observations:

- the presence of randomly-aligned Al_3Ti
- the consumption of the initial Ti-layer
- the presence of epitaxial layer in direct contact with the barrier.

The obtained results in this paper illustrate that the interaction between the nitride layers and the metallic contact **creates a peculiar**[64] crystal alignment of the metallic contacts. As the contact resistances can **be lowered by either optimising the contact stack as well as optimising the barrier**[65], it is clear that a similar contact stack alone is not sufficient to obtain a low-resistive contact on various nitride semiconductors. Further optimisation of the advanced AlN or even $In_yAl_{1-y}N$-barriers will be required for the enhancement of the electron tunnelling through the barrier.

ACKNOWLEDGMENTS

The research activities were carried out within the project *InRel-NPower*, which has received funding from the European Union's Horizon 2020 research and innovation programme under grant agreement No. 720527.

This research used resources of the DiffAbs beamline under guidance of C. Mocuta at the SOLEIL synchrotron, France. We acknowledge the SOLEIL Synchrotron, France, for granting the beamtime for these experiments. We would like to thank Ph. Joly for technical assistance. Raw data were generated at the SOLEIL synchrotron. Derived data supporting the findings of this study are available from the corresponding author upon reasonable request.

V. ADDENDUM

A. Plotting of orientation-resolved X-ray diffraction

An XRD *pole figure* displays, in polar coordinates elevation angle χ and azimuth angle ϕ, the recorded diffracted intensity for a specific diffraction angle 2θ. For example, Fig. 2a shows the polar plot of the diffraction near the Si(220) and GaN(102) planes (d = 1.92Å and 1.89 Å, respectively) of a bare $Al_xGa_{1-x}N$-based heterostructure. The spots of higher intensity (yellow) indicate that the observed planes are oriented at those very specific angles. The observed elevation χ angles correspond with the typical geometric angles in the crystal unit cell of Si and GaN. Table I contains useful crystalline data for the epitaxial Si and GaN diffraction. Since GaN(002)//Si(111), the inclination angle for all other diffraction planes can be calculated from the reported crystal unit cells. Note that these figures can also be used to evaluate preferential crystal orientations, such as a random alignment or a fibre alignment, which would result in a uniformly-increased intensity or a concentric ring of higher intensity, respectively. A fibre alignment is a preferential orientation where all grains share a fixed orientation of a specific plane, which is always parallel to the samples' surface. Individual crystal grains can still rotate freely along the normal of this plane. A single pole figure would contain concentric circles, where the radius of the concentric circle corresponds with the elevation angle χ between the diffracting plane and the plane that is the rotation axis.

An XRD *color plot* (Fig. 2b) is obtained by averaging the recorded intensities of a single pole-figure over the in-plane rotation angle ϕ, and was previously introduced by Gaudet et al.[66]. As such, one obtains an averaged intensity value for every concentric circle on the pole figure with equal elevation angles χ. By calculating these averaged values for every value of χ and 2θ, one obtains a two-dimensional colorplot such as displayed in the bottom part of Fig. 2b. In this graphical representation one can perform standard XRD phase identification by determining the positions of higher diffracted intensity as a function of 2θ. In addition, these diffraction maps can also be used to investigate the alignment of randomly, epitaxially, or fibre-oriented compounds. A *randomly* aligned sample would diffract at specific values of diffraction angle 2θ and for every value of elevation angle χ. The diffraction color map would therefore display vertical lines at these 2θ positions. A highly-textured, *epitaxial* film would only diffract at specific, and well defined, regions in diffraction angles 2θ, elevation angle χ and azimuth ϕ. The corresponding diffraction

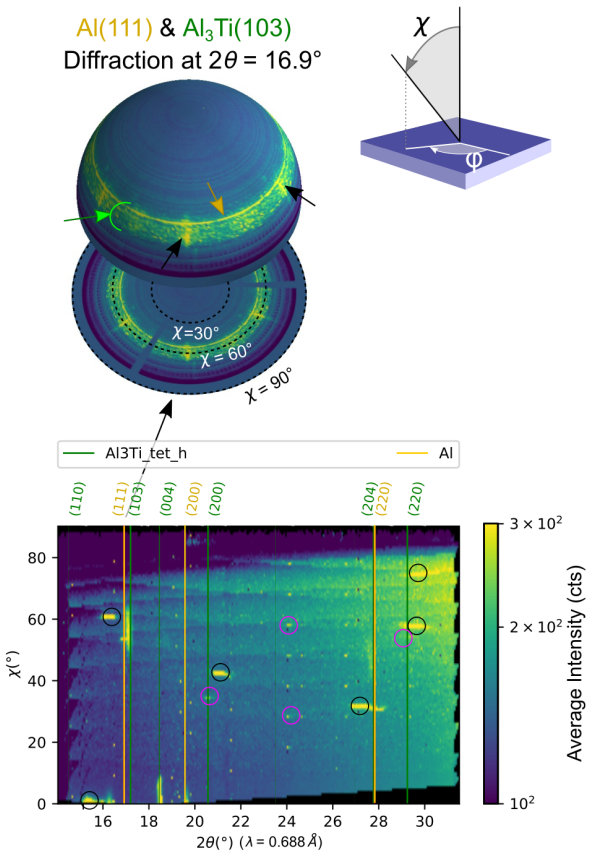

FIG. 20: X-ray diffraction intensities of an annealed Ti-Al-TiN contact stack on a $Al_xGa_{1-x}N$ heterostructure. The contact with 16 at.%Ti was annealed up to 700 °C. (top) The diffraction intensities of both Si(220) and GaN(102) planes while tilting the sample both in- and out-of-plane for a fixed diffraction angle. (bottom) The diffraction intensities as a function of diffraction angle and the sample's out-of-plane tilt (the displayed intensities were averaged along the in-plane tilting angle).

maps therefore contains only local spots of higher intensity as a function of 2θ and χ (e.g. Fig. 2). Finally, one can also observe *fiber* orientation: an XRD color plot of a fibre texture will also correspond to local spots at specific 2θ and χ angles (Fig. 20).

REFERENCES

[1]H. Amano, Y. Baines, E. Beam, M. Borga, T. Bouchet, P. R. Chalker, M. Charles, K. J. Chen, N. Chowdhury, R. Chu, *et al.*, "The 2018 GaN power electronics roadmap," Journal of Physics D: Applied Physics **51**, 163001 (2018).

[2]G. Greco, F. Iucolano, and F. Roccaforte, "Ohmic contacts to gallium nitride materials," Applied Surface Science **383**, 324–345 (2016).

[3]Y. Takei, K. Tsutsui, W. Saito, K. Kakushima, H. Wakabayashi, and H. Iwai, "Dependence of ohmic contact properties on AlGaN layer thickness for AlGaN/GaN high-electron-mobility transistors," Japanese Journal of Applied Physics **55**, 040306 (2016).

[4]Original text: A comparative study is therefore required on the performance of low-resistive ohmic contacts on different nitride-based barriers. To understand the formation of ohmic contacts, one requires to control and systematically investigate the many parameters that influence its fabrication process, such as annealing conditions, initial composition of the metal stack and protective capping layer.

[5]Original text: Elements with a low metal work function such as Ti, Ta or Al have been amongst the most reported materials for ohmic contact formation on $Al_xGa_{1-x}N$/GaN heterostructures.

[6]A. Constant, J. Baele, P. Coppens, W. Qin, H. Ziad, E. De Backer, P. Moens, and M. Tack, "Impact of Ti/Al atomic ratio on the formation mechanism of non-recessed Au-free ohmic contacts on AlGaN/GaN heterostructures," Journal of Applied Physics **120**, 104502 (2016).

[7]D. W. Seo, H. G. Choi, J. Twynam, K. M. Kim, J. S. Yim, S.-W. Moon, S. Jung, J. Lee, and S. D. Roh, "600 V-18 A GaN Power MOS-HEMTs on 150 mm Si Substrates With Au-Free Electrodes," IEEE Electron Device Letters **35**, 446–448 (2014).

[8]M. Van Hove, X. Kang, S. Stoffels, D. Wellekens, N. Ronchi, R. Venegas, K. Geens, and S. Decoutere, "Fabrication and Performance of Au-Free AlGaN/GaN-on-Silicon Power Devices With Al2O3 and Si3N4 / Al2O3 Gate Dielectrics," IEEE Transactions on Electron Devices **60**, 3071–3078 (2013).

[9]S. N. Mohammad, "Contact mechanisms and design principles for alloyed ohmic contacts to n-GaN," Journal of Applied Physics **95**, 7940–7953 (2004).

[10]A protective capping layer is then also required to prevent out-diffusion and undesired oxidation of the top metallization.

[11]Most.

[12]H. Lee, D. Lee, and T. Palacios, "AlGaN/GaN high-electron-mobility transistors fabricated through a Au-free technology," IEEE Electron Device Letters **32**, 623–625 (2011).

[13]J. Zhang, S. Huang, Q. Bao, X. Wang, K. Wei, Y. Zheng, Y. Li, C. Zhao, X. Liu, Q. Zhou, *et al.*, "Mechanism of Ti/Al/Ti/W Au-free ohmic contacts to AlGaN/GaN heterostructures via pre-ohmic recess etching and low temperature annealing," Applied Physics Letters **107**, 262109

(2015).

[14]B. De Jaeger, M. Van Hove, D. Wellekens, X. Kang, H. Liang, G. Mannaert, K. Geens, and S. Decoutere, "Au-free CMOS-compatible AlGaN/GaN HEMT processing on 200 mm Si substrates," in *2012 24th International Symposium on Power Semiconductor Devices and ICs* (IEEE, 2012) pp. 49–52.

[15]A. Firrincieli, B. De Jaeger, S. You, D. Wellekens, M. Van Hove, and S. Decoutere, "Au-free low temperature ohmic contacts for AlGaN/GaN power devices on 200 mm Si substrates," Japanese Journal of Applied Physics **53**, 04EF01 (2014).

[16]Z. Liu, S. Arulkumaran, and G. Ng, "Temperature dependence of ohmic contact characteristics in algan/gan high electron mobility transistors from- 50 to 200 c," Applied physics letters **94**, 142105 (2009).

[17]H. Huang, Y. C. Liang, G. S. Samudra, and C. L. L. Ngo, "Au-free normally-off AlGaN/GaN-on-Si MIS-HEMTs using combined partially recessed and fluorinated trap-charge gate structures," IEEE Electron Device Letters **35**, 569–571 (2014).

[18]Rearrangement of sentences.

[19]B. Van Daele, G. Van Tendeloo, W. Ruythooren, J. Derluyn, M. Leys, and M. Germain, "The role of al on ohmic contact formation on n-type gan and algan/ gan," Applied Physics Letters **87**, 061905 (2005).

[20]We demonstrated that the Ti-Al ratio is the key parameter defining the optimum annealing temperature for ohmic contact formation[6], in corroboration with earlier insights on similar metal contact schemes[19].

[21]M. Sujata, S. Bhargava, and S. Sangal, "On the formation of TiAl3 during reaction between solid Ti and liquid Al," Journal of materials science letters **16**, 1175–1178 (1997).

[22]For each Ti-Al ratio an optimum annealing temperature exists.

[23]As most papers are limited in either (or even both) the number of samples with different Ti-to-Al ratios in the metal stack, or the number of annealing temperatures, a systematic study which enables direct comparison of these contact stacks as function of Ti-to-Al ratio, annealing temperature and of the heterostructure barriers is not available.

[24]The investigation of the formed crystal structures allows to identify the contact compositions that correlate with the best performing ohmic contacts.

[25]GaN-based heterostructures.

[26]W. Devulder, K. Opsomer, J. Meersschaut, D. Deduytsche, M. Jurczak, L. Goux, and C. Detav-

ernier, "Combinatorial study of Ag–Te thin films and their application as cation supply layer in CBRAM cells," ACS combinatorial science **17**, 334–340 (2015).

[27]These wafers.

[28]A small out-of-plane tilt of the sample of only a few degrees was introduced so the obtained XRD-measurements do not include the highly-intense GaN(002) diffraction peak, in order to prevent over-exposure of the detector.

[29]R. T. Tung, J. Poate, J. Bean, J. Gibson, and D. Jacobson, "Epitaxial silicides," MRS Online Proceedings Library Archive **10** (1981).

[30]B. De Schutter, K. De Keyser, C. Lavoie, and C. Detavernier, "Texture in thin film silicides and germanides: a review," Applied Physics Reviews **3**, 031302 (2016).

[31]In contrast with (high-resolution) transmission electron microscopy (TEM) imaging, which would evaluate the crystalline alignment of a very small area (order of 100 nm), XRD-pole figures are able to evaluate the crystalline alignment of an area of the X-ray footprint, e.g. order of 100 µm).

[32]C. Mocuta, M. Richard, J. Fouet, S. Stanescu, A. Barbier, C. Guichet, O. Thomas, S. Hustache, A. Zozulya, and D. Thiaudiere, "Fast pole figure acquisition using area detectors at the DiffAbs beamline–Synchrotron SOLEIL," Journal of Applied Crystallography **46**, 1842–1853 (2013).

[33]P. Pangaud, S. Basolo, N. Boudet, J.-F. Berar, B. Chantepie, P. Delpierre, B. Dinkespiler, S. Hustache, M. Menouni, and C. Morel, "XPAD3: A new photon counting chip for X-ray CT-scanner," Nuclear Instruments and Methods in Physics Research Section A: Accelerators, Spectrometers, Detectors and Associated Equipment **571**, 321–324 (2007).

[34]P. Pangaud, S. Basolo, N. Boudet, J.-F. Berar, B. Chantepie, J.-C. Clemens, P. Delpierre, B. Dinkespiler, K. Medjoubi, S. Hustache, *et al.*, "XPAD3-S: A fast hybrid pixel readout chip for X-ray synchrotron facilities," Nuclear Instruments and Methods in Physics Research Section A: Accelerators, Spectrometers, Detectors and Associated Equipment **591**, 159–162 (2008).

[35]K. Medjoubi, T. Bucaille, S. Hustache, J.-F. Bérar, N. Boudet, J.-C. Clemens, P. Delpierre, and B. Dinkespiler, "Detective quantum efficiency, modulation transfer function and energy resolution comparison between CdTe and silicon sensors bump-bonded to XPAD3S," Journal of Synchrotron Radiation **17**, 486–495 (2010).

[36]K. Medjoubi, A. Thompson, J.-F. Bérar, J.-C. Clemens, P. Delpierre, P. Da Silva, B. Dinkespiler, R. Fourme, P. Gourhant, B. Guimaraes, *et al.*, "Energy resolution of the CdTe-XPAD detector: calibration and potential for Laue diffraction measurements on protein crystals," Journal of

Synchrotron Radiation **19**, 323–331 (2012).

[37]A. Shriki, R. Winter, Y. Calahorra, Y. Kauffmann, G. Ankonina, M. Eizenberg, and D. Ritter, "Formation mechanism of gold-based and gold-free ohmic contacts to AlGaN/GaN heterostructure field effect transistors," Journal of Applied Physics **121**, 065301 (2017).

[38]S. Lenci, B. De Jaeger, L. Carbonell, J. Hu, G. Mannaert, D. Wellekens, S. You, B. Bakeroot, and S. Decoutere, "Au-free AlGaN/GaN power diode on 8-in Si substrate with gated edge termination," IEEE Electron Device Letters **34**, 1035–1037 (2013).

[39]G. El-zammar, A. Yvon, W. Khalfaoui, M. Nafouti, F. Cayrel, E. Collard, and D. Alquier, "A simple non-recessed and Au-free high quality Ohmic contacts on AlGaN/GaN: The case of Ti/Al alloy," Materials Science in Semiconductor Processing **78**, 107–110 (2018).

[40]J. Zhang, X. Kang, X. Wang, S. Huang, C. Chen, K. Wei, Y. Zheng, Q. Zhou, W. Chen, B. Zhang, *et al.*, "Ultralow-Contact-Resistance Au-Free Ohmic Contacts With Low Annealing Temperature on AlGaN-GaN Heterostructures," IEEE Electron Device Letters **39**, 847–850 (2018).

[41]And includes data from this study as well as literature.

[42]To further explore the above classification in two region-of-interest, we investigated the phase formation, crystal structure and crystal-orientation of the Ti-Al-TiN stacks on $Al_xGa_{1-x}N$, AlN, GaN and $In_yAl_{1-y}N$ layers.

[43]The diffraction patterns of two measurements are displayed in Figs. 4 and 5 for respectively 16 and 29 at.% Ti, two concentrations that are representative for the two main phase sequences observed for the Ti-Al-TiN contact stack.

[44]Show the as-deposited layers at room temperature of a stack with 16 at.% Ti. A TiN(111) peak is observed near 2θ=36.8°, and the peak near 2θ=38.5° can be related to both Ti(002) and Al(111) (see also section III C 1 for an in-depth discussion based on XRD pole figures), two crystal planes that have coinciding diffraction peaks due to a similar crystal plane spacing.

[45]The diminishing.

[46]*Binary Alloy Phase Diagrams* (ASM international, 1996).

[47]J. Schuster and M. Palm, "Reassessment of the binary aluminum-titanium phase diagram," Journal of phase equilibria and diffusion **27**, 255–277 (2006).

[48]By discussing the measurements more detailed, some interesting observations can be made.

[49], corroborating that a liquid of Al is present.

[50]With a different orientation.

[51]G. Lemperiere and J. Poitevin, "Influence of the nitrogen partial pressure on the properties of

dc-sputtered titanium and titanium nitride films," Thin Solid Films **111**, 339–349 (1984).

[52]L. Meng and M. Dos Santos, "Characterization of titanium nitride films prepared by dc reactive magnetron sputtering at different nitrogen pressures," Surface and Coatings Technology **90**, 64–70 (1997).

[53]Stability of the formed contact.

[54], above which the presence of epitaxial Al, as well as the integrity of the TiN capping layer is destroyed.

[55]At higher temperatures now no remaining Al is observed above.

[56], but at sufficiently high temperatures so that Ti is already consumed and has formed Al_3Ti and where Al did not yet form a liquid phase.

[57]At those diffraction angles of Ti, Al and TiN planes, we observe that also here the diffraction is limited at specific values of elevation angle χ, indicating a preferential orientation.

[58], equal to their inclination angle to the Al(111) plane as defined by the crystal structure of Al.

[59]Layer.

[60]Two types of preferential orientations are possible: epitaxial-alignment and fibre-alignment, one needs to take a closer look to the individual pole figures, as displayed in Fig. 11.

[61]V. Garbe, J. Weise, M. Motylenko, W. Munchgesang, A. Schmid, D. Rafaja, B. Abendroth, and D. Meyer, "Au-free ohmic Ti/Al/TiN contacts to UID n-GaN fabricated by sputter deposition," Journal of Applied Physics **121**, 065703 (2017).

[62]As this metal stack has formed randomly-aligned Al_3Ti after the consumption of the initial Ti-layer, but did not form a low-resistive ohmic contact, one can reference in section III C 2 that the presence of epitaxial Al seems to be a critical difference that results in the formation of a low-resistive ohmic contact.

[63]Again we observe that the formation of a low-resistive ohmic contact occurs when the presence of randomly-aligned Al_3Ti , and the consumption of the initial Ti-layer is combined with the presence of an epitaxial layer, this time the Ti_2AlN layer as an interface layer between the barrier and Al_3Ti. The Ti_2AlN layers have an epitaxial alignment, where the a- and c-axes of Ti_2AlN align in orientation with the same axes of $Al_xGa_{1-x}N$.

[64]Is highly interacting with the.

[65]Be influenced by changing the barrier composition and thickness.

[66]S. Gaudet, P. Desjardins, and C. Lavoie, "The thermally-induced reaction of thin Ni films with Si: Effect of the substrate orientation," Journal of Applied Physics **110**, 113524 (2011).

[67]H. Sun, M. Liu, P. Liu, X. Lin, J. Chen, M. Wang, and D. Chen, "Optimization of Au-Free Ohmic Contact Based on the Gate-First Double-Metal AlGaN/GaN MIS-HEMTs and SBDs Process," IEEE Transactions on Electron Devices **65**, 622–628 (2017).

[68]W. Jatal, U. Baumann, K. Tonisch, F. Schwierz, and J. Pezoldt, "High-frequency performance of GaN high-electron mobility transistors on 3C-SiC/Si substrates with Au-free ohmic contacts," IEEE Electron Device Letters **36**, 123–125 (2014).

[69]J. Hu, S. Stoffels, S. Lenci, T.-L. Wu, N. Ronchi, S. You, B. Bakeroot, G. Groeseneken, and S. Decoutere, "Investigation of constant voltage off-state stress on Au-free AlGaN/GaN Schottky barrier diodes," Japanese Journal of Applied Physics **54**, 04DF07 (2015).

[70]B. De Schutter, K. De Keyser, and C. Detavernier, "Visualization and classification of epitaxial alignment at hetero-phase boundaries," Thin Solid Films **599**, 104–112 (2016).